Journal of ELECTRONIC MATERIALS, Vol. 46, No. 4, 2017
DOI: 10.1007/s11664-017-5346-7

Electrical Properties of MWCNT/HDPE Composite-Based MSM Structure Under Neutron Irradiation

H. KASANI,[1] R. KHODABAKHSH,[2] M. TAGHI AHMADI,[3,6] D. REZAEI OCHBELAGH,[4] and RAZALI ISMAIL[5]

1.—Department of Physics, Faculty of Sciences, University of Mohaghegh Ardabili, Ardabil, Iran. 2.—Department of Physics, Faculty of Sciences, Urmia University, Urmia, Iran. 3.—Nano-technology Research Center, Nano-Electronic Group, Physics Department, Urmia University, Urmia, Iran. 4.—Departments of Nuclear Engineering and Physics, Amirkabir University of Technology, Tehran, Iran. 5.—Department of Electronics and Computer Engineering, Faculty of Electrical Engineering, Universiti Teknologi Malaysia, UTM Johor Bahru, 81310 Johor, Malaysia. 6.—e-mail: mohammad.ahmadi1351@gmail.com

Because of their low cost, low energy consumption, high performance, and exceptional electrical properties, nanocomposites containing carbon nanotubes are suitable for use in many applications such as sensing systems. In this research work, a metal–semiconductor–metal (MSM) structure based on a multiwall carbon nanotube/high-density polyethylene (MWCNT/HDPE) nanocomposite is introduced as a neutron sensor. Scanning electron microscopy, Fourier-transform infrared, and infrared spectroscopy techniques were used to characterize the morphology and structure of the fabricated device. Current–voltage (I–V) characteristic modeling showed that the device can be assumed to be a reversed-biased Schottky diode, if the voltage is high enough. To estimate the depletion layer length of the Schottky contact, impedance spectroscopy was employed. Therefore, the real and imaginary parts of the impedance of the MSM system were used to obtain electrical parameters such as the carrier mobility and dielectric constant. Experimental observations of the MSM structure under irradiation from an americium–beryllium (Am–Be) neutron source showed that the current level in the device decreased significantly. Subsequently, current pulses appeared *in situ* I–V and current–time (I–t) curve measurements when increasing voltage was applied to the MSM system. The experimentally determined depletion region length as well as the space-charge-limited current mechanism for carrier transport were compared with the range for protons calculated using Monte Carlo n-particle extended (MCNPX) code, yielding the maximum energy of recoiled protons detectable by the device.

Key words: MWCNT/HDPE nanocomposite, electrical properties, neutron irradiation, proton recoil, HDPE, neutron detection

INTRODUCTION

Recent years have witnessed great interest in micro- and nanostructured semiconductor materials for use in sensors, electronic devices, and catalysts.[1] Various methods have been developed for synthesis of nanostructured electronic devices and nanocomposites in the hope of designing and fabricating radiation sensors, ultraviolet (UV) photodetectors, and various optical devices.[2,3]

Measurement of the energy of fast neutrons is very important in various research fields such as nuclear physics, advanced nuclear technology, medical diagnosis, radiotherapy, and radiation protection. Recently, carbon-based materials have been

(Received November 28, 2016; accepted January 31, 2017; published online February 13, 2017)

used in many applications such as sensors, nanoelectronics, optical switches, etc. due to their unique electrical, thermal, and mechanical properties.[4–6] Specifically, many studies have been conducted to investigate CNT/polymer composites.[7–10] Moreover, their application in nanoelectronic sensors has been explored because of their rapid and sensitive response.[11] Originally, in this regard, analysis of charged particle radiation is necessary to investigate the properties of nanoelectronic devices in many applications, especially in outer space conditions and for radiation detection systems.[12–17] Recently, graphene field-effect transistors and ^{10}B-based converters have been used as a radiation detection platform and for thermal neutron detection.[18,19]

On the other hand, materials with low atomic number such as hydrogen are desirable candidates for fast neutron detection applications because of their high elastic scattering cross-section for fast neutrons.[20] Hydrogenous materials, such as polyethylene, undergo (n, p) reactions from fast neutrons, generating recoiled protons which are detectable by common charged particle detectors.[21,22]

Conventional semiconductor-based detectors are common devices for radiation detection. Most such detectors are made of silicon and germanium, and their main feature is high energy resolution compared with other radiation detectors.[23] Furthermore, these detectors have many advantages such as compactness, low weight, simple operation, and low applied voltage, compared with gas chambers or scintillation techniques. In this study, polyethylene as a converter layer and carbon-based composite as a charged particle detector were employed based on back-to-back Schottky diodes in a metal–semiconductor–metal (MSM) structure. Since high-density polyethylene (HDPE) has semiconducting properties, it has been widely used in organic electronics,[24] so it seems that the fast neutron detector platform demonstrated herein can be categorized as an organic electronic device as well. Under exposure to irradiation from an americium–beryllium (Am–Be) neutron source, the current–voltage (I–V) characteristics of the fabricated device were measured *in situ*. The results showed that the electrical characteristics of the proposed fast neutron detector device, such as the I–V and current–time (I–t) curves, changed during and after neutron irradiation.

FABRICATION AND CHARACTERISTICS

Arc discharge is the oldest technique to produce carbon nanotubes (CNTs) in bulk, first used by Iijima in 1991. This method has also been developed for use in polyethylene glycol solution as liquid medium with graphite electrodes.[25] As shown in Fig. 1, in the present work, the arc discharge method with two copper (Cu) electrodes in molten HDPE was used. Note that the high-voltage generator is connected to copper electrodes mounted in molten HDPE, and this setup is placed on a glass sheet where the HDPE is heated by a heating system. The distance between the electrodes (channel length, L) was about 680 μm.

After the growth process, I–V measurements were carried out using a BHP-2064 electrochemical analysis system by the two-probe method, using a counting and reference probe and another as the working probe.

The morphological properties were characterized by scanning electron microscopy (SEM). Figure 2 shows SEM images of the synthesized sample at different magnifications.

According to the SEM images, it is concluded that the CNTs were coated with HDPE (Fig. 2a), similar to the composites presented in Ref. 26. Also, Fig. 2c shows that bundled multiwall carbon nanotubes (MWCNTs) were coated by HDPE chains, where the mechanism of formation is similar to the process explained in Ref. 27.

To investigate the functionalization of the composite, infrared (IR) and Fourier-transform infrared (FTIR) analyses were used. In this method, IR radiation is focused on the sample and its absorption (or transmittance) observed, which is a quantized process. It is clear that two molecules do not have exactly the same IR spectrum. The infrared spectrum of the synthesized sample was obtained using a Shimadzu IR spectrometer in the wavenumber range from 500 cm^{-1} up to 4000 cm^{-1} using potassium bromide (KBr) pellets. To show that the synthesized sample was a composite of MWCNTs and HDPE, their FTIR spectra were investigated and compared with the IR spectrum of the sample used in this work.

The signals at 2926 cm^{-1} and 2853 cm^{-1} in Fig. 3a correspond to modes of CH_2 group in hydrocarbons. Similarly, it is well recognized that CH_2 vibration produces absorption at about 1460 cm^{-1}. So, the strong peak at about 1460 cm^{-1} for polyethylene is due to bending mode of CH_2 group. Also, the rocking mode of CH_2 group gives rise to the intense peak in the spectrum near 725 cm^{-1}.[28] The peak at 3443 cm^{-1} in the FTIR spectrum of the MWCNTs (Fig. 3d) can be ascribed to O–H vibration in carboxyl group.[29,30] The peaks appearing in the region between 1640 cm^{-1} and 1670 cm^{-1} can be attributed to stretching of the CNT backbone and carboxyl groups.[31] These results clearly establish that the IR spectrum of the synthesized sample (Fig. 3b) is the combination of those in Fig. 3a and d.

EXPERIMENTAL PROCEDURES

Device Modeling

A semiconductor with two metal contacts on opposite sides is introduced as an MSM structure, with operation and performance related to the

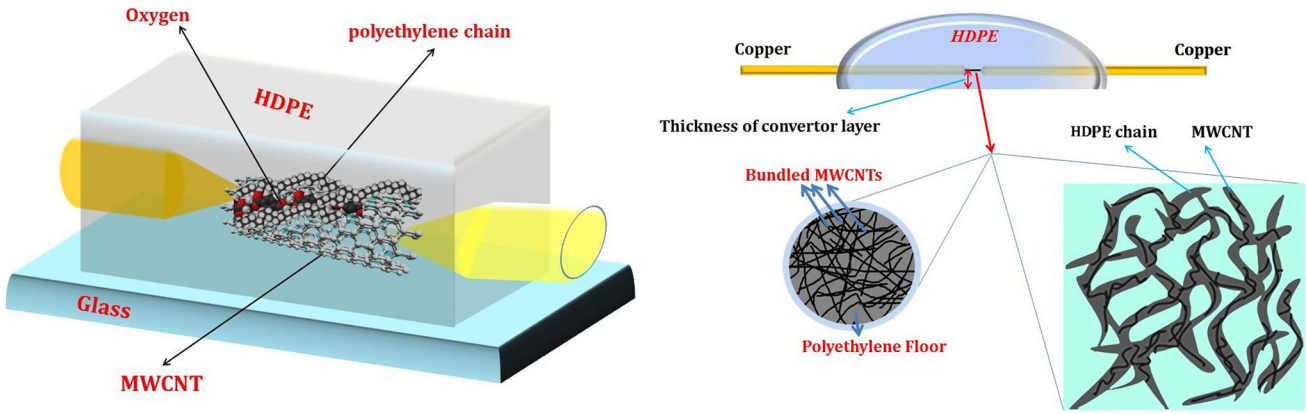

Fig. 1. Schematic of fabricated MWCNT/HDPE composite-based Schottky diode.

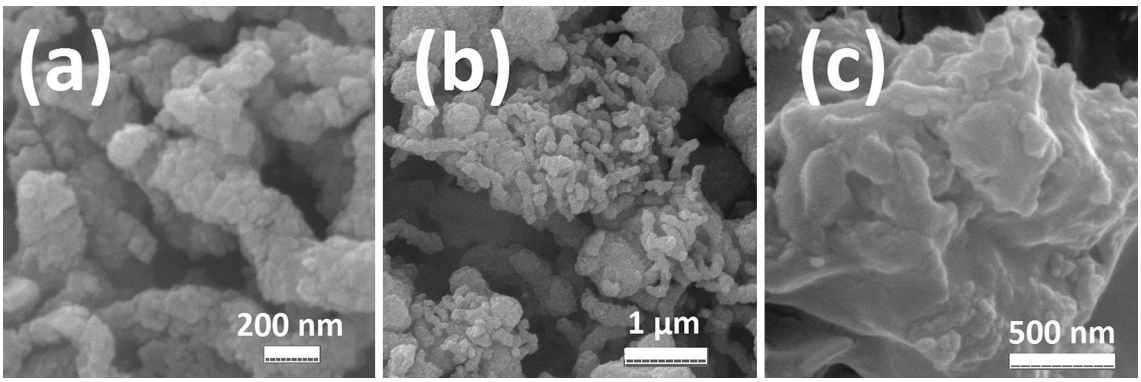

Fig. 2. SEM images of (a) cylindrical nanoparticles seen in (b), and (c) bulk nanoparticles in the synthesized sample.

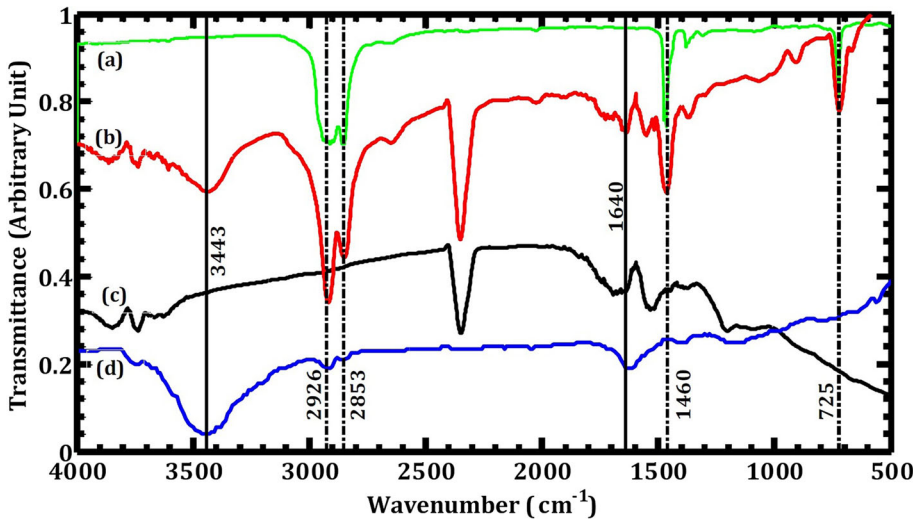

Fig. 3. (a) FTIR spectrum of polyethylene, (b) IR spectrum of synthesized sample, (c) background, and (d) FTIR spectrum of pristine MWCNTs.

contact types. In literature, Schottky contacts in the MSM system are known as back-to-back Schottky diodes.[32] In this work, the MSM system was modeled as two Schottky barriers connected back-to-back. This back-to-back Schottky model under the assumptions of thermionic emission theory was used for the carbon-based MSM system. Using thermionic emission theory, the current at a specific temperature, T, for barriers 1 and 2 can be written as[33]

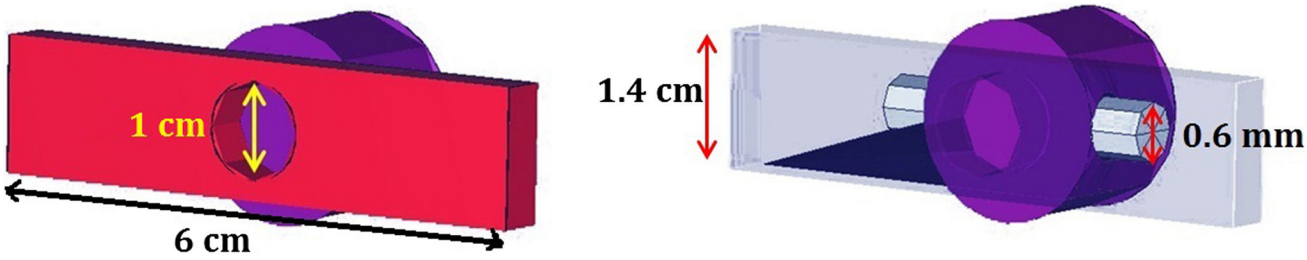

Fig. 4. Scheme of MWCNT/HDPE nanocomposite Schottky diode-based detector platform.

$$I_1 = I_{s1}\left[exp(\frac{qV_1}{nk_BT})-1\right], \quad (1)$$

$$I_2 = -I_{s2}\left[exp(-\frac{qV_2}{nk_BT})-1\right], \quad (2)$$

where $I_{s1,s2} = ART^2 \exp\left(-\frac{q\Phi_{B1,B2}}{k_BT}\right)$, R is the Richardson constant, A is the area of the contact cross-section, Φ_{B1} and Φ_{B2} are the Schottky barrier heights, q is the electron elementary charge, and k_B is the Boltzmann constant. Nevertheless, surface disorder and random surface states also affect the Schottky barrier formation in both junctions, resulting in deviation of the barrier height from the ideal Schottky barrier. The latter effect is determined by a dimensionless parameter called the identity factor, n. Also, image-force effects should be considered, resulting in voltage dependence of the barrier heights as given in Ref. 32:

$$\Phi_{B1}=\Phi_{B01} + V_1\left(\frac{1}{n_{if}}-1\right), \quad (3a)$$

$$\Phi_{B2}=\Phi_{B02} + V_2\left(\frac{1}{n_{if}}-1\right), \quad (3b)$$

where n_{if} is a dimensionless parameter, Φ_{B01} and Φ_{B02} are the zero-bias barrier height values, and V_1 and V_2 are the voltages applied on barrier 1 and 2, respectively. Other effects such as tunneling currents or generation–recombination in the depletion region should be included in Eq. 3 as well as. According to the current continuous theory, the total current I across the device is $I = I_1 = I_2$, setting $V = V_1 + V_2$. Therefore, the I–V relationship for the MSM system with two Schottky contacts is

$$I(V) = \frac{2I_{s1}I_{s2}\sinh\left(\frac{qV}{2nk_BT}\right)}{I_{s1}\exp\left(\frac{qV}{2nk_BT}\right) + I_{s2}\exp\left(\frac{-qV}{2nk_BT}\right)}. \quad (4)$$

It is important to mention that the reverse bias V_2 can be replaced by the forward bias V_1 on switching the current direction. Therefore, a symmetrical I–V curve is obtained when using two identical metals. Additionally, another improved approach for analysis of the MSM system was presented in Ref. 34. The modeling results indicated that the reverse-biased voltage V_2 along the MSM system is relatively larger and constant compared with V_1. As a result, the calculated value of the depletion layer length, obtained from impedance spectroscopy results (see Sect. 6), is mainly related to the reverse-biased junction, so the device can be roughly considered to be a reverse-biased Schottky diode, which is the purpose of I–V modeling.

Experimental Setup

The experimental setup and method used to measure the response of the MSM system to neutrons from the Am–Be neutron source at room temperature were as follows: Firstly, the sample separated from the glass substrate (Fig. 1) was attached to a HDPE sheet with a circular hole as a window for the proposed detector (Fig. 4).

The sample was then placed in a hole formed in the outer wall of a polyethylene cylindrical shell (Fig. 5). Meanwhile, the neutron source was placed at the center of the cylindrical shell so that neutrons would pass through the hole and collide with the device. Additionally, the distance from the detector to the source was about 12 cm, as shown in Fig. 5.

In the next step, when the setup was completed, I–V and I–t measurements were carried out by linear sweep voltammetry and chronoamperometry methods, respectively.

Monte Carlo Simulation

In this work, Monte Carlo n-particle extended (MCNPX) code was used to simulate the effect of neutron irradiation on the MSM system and to optimize the thickness of the HDPE converter layer for the Am–Be neutron source. A volumetric and isotropic ^{241}Am–^{9}Be neutron source was considered in the MCNPX code. The ^{241}Am–^{9}Be neutron source has a relatively long half-life (432.7 years), in which ^{241}Am is an alpha particle emitter and generates neutrons through the ^{9}Be(α,n)^{12}C reaction.[23] This reaction has several neutron and photon channels,[35] with 4.438-MeV gamma rays being the most important in the gamma channel, since 60% of generated neutrons are emitted in coincidence with 4.438 MeV gamma-rays.[36,37] However, the effects of gamma rays can be ignored in this situation. It is important

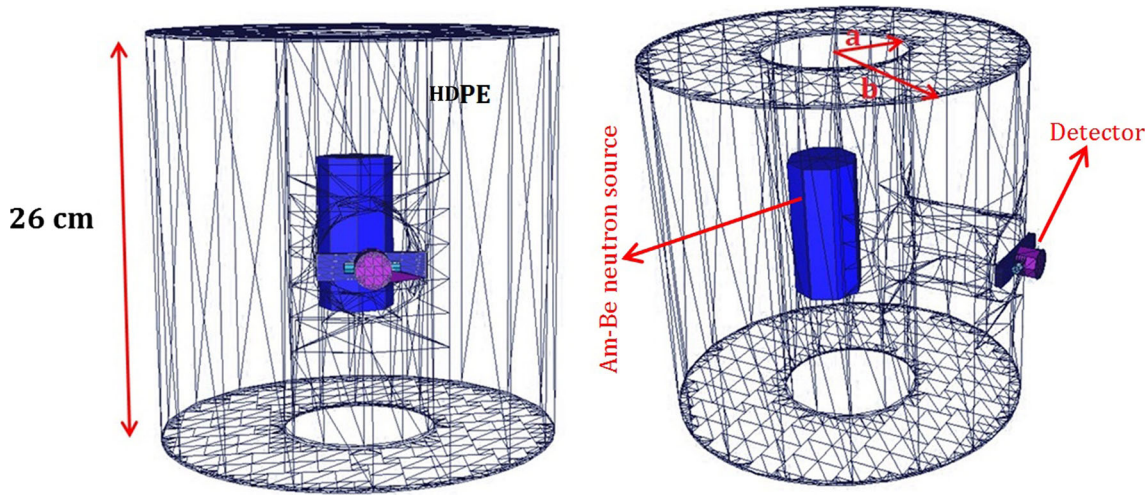

Fig. 5. Scheme of detector exposure method (a = 5 cm, b = 13 cm).

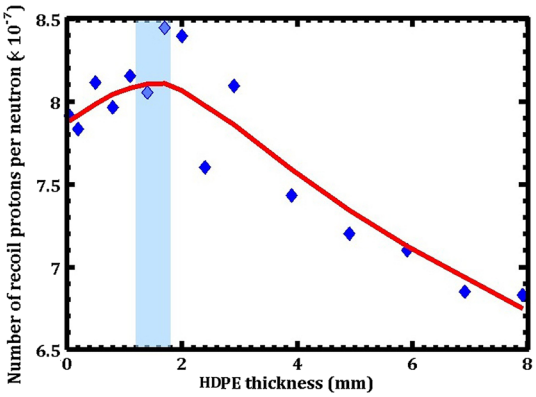

Fig. 6. Number of recoiled protons as function of HDPE converter thickness.

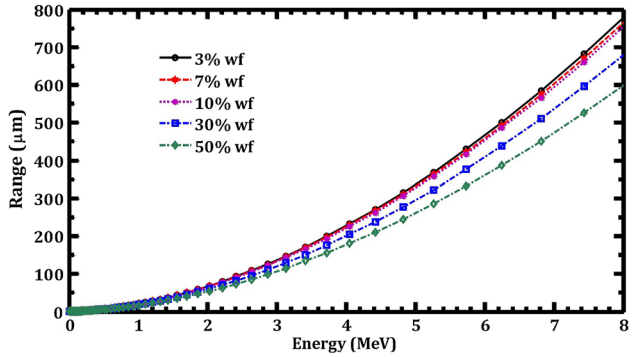

Fig. 7. Range–energy curves for protons in MWCNT/HDPE composite with different weight fractions (wf) of MWCNTs.

to mention that the activity of the source is about 5 curie (Ci).[38]

The MCNPX code includes transport of not only neutrons but also recoiled protons in all energy ranges. Recoiled protons pass through the HDPE layer, where some of them are stopped, while others subsequently reach the active volume of the Schottky contact. The optimum thickness of the HDPE converter layer was calculated using the F1 tally, i.e., the number of recoiled protons per neutron, as a function of converter thickness. The optimum value of the HDPE thickness was about 1.5 mm, as shown in Fig. 6.

The relationship between the range of protons in the MWCNT/HDPE composite with different weight fractions of MWCNT and their energies is presented in Fig. 7. As expected, it can be seen that increasing the weight fraction of MWCNTs in the composite resulted in reduced proton range at given energy. This means that the maximum energy of the recoiled protons deposited in the depletion region increased at higher MWCNT fraction. We should also point out that the greatest portion of the proton energy is deposited at the end of the path, which can be described by the Bragg curve of the proton.[39]

Depletion Region Considerations

The depletion width W in a Schottky contact can be determined by Poisson's equation as[33]

$$W = \sqrt{\frac{2\varepsilon_0 \varepsilon}{qN}(V_{\mathrm{bi}} - V_{\mathrm{A}})}, \tag{5}$$

where ε_0 is the vacuum permittivity, ε is the relative permittivity of the semiconductor, V_{bi} is the built-in voltage, N is the dopant density, q is the electron charge, and V_{A} is the voltage applied across the Schottky contact in forward bias. To obtain the depletion width, the capacitance across the diode should be measured in different biases. The slope of the C^{-2} versus V curve gives the built-in voltage and doping density.[40] This capacitance measurement method is commonly used to obtain the depletion width in Schottky contacts. Unfortunately, capacitance measurements on organic Schottky junctions

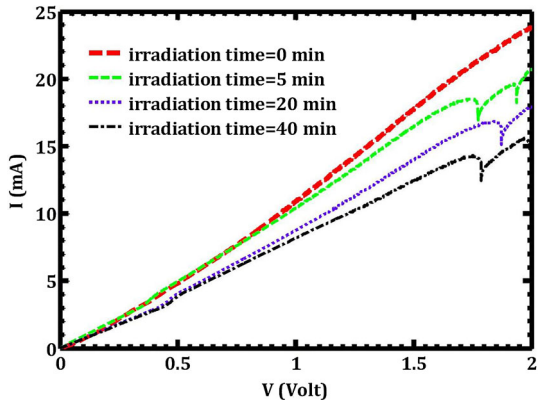

Fig. 8. *I–V* characteristics for different neutron irradiation durations.

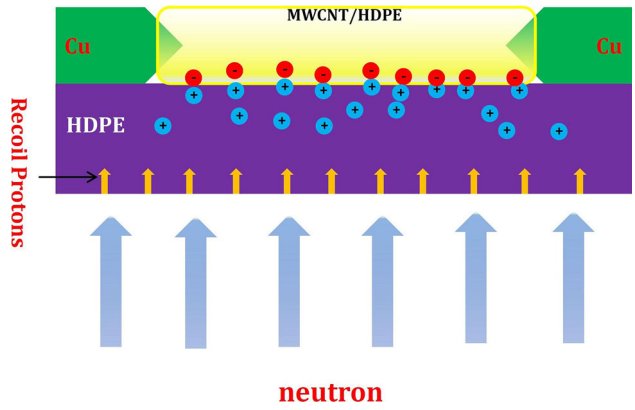

Fig. 9. Scheme of combination process of conduction electrons with positive trap charges at the HDPE/(MWCNT/HDPE) interface.

are challenging due to their unique properties,[41] thus V_{bi} and N were estimated. In the framework of Schottky emission for a metal–semiconductor contact, V_{bi} can be estimated from the *I–V* curve using the relation[42]

$$\ln(J) = b(V + V_{bi})^{1/4}, \tag{6}$$

where b and V_{bi} are fitting parameters and J is the current density. Meanwhile, N can be obtained from $\sigma = qN\mu$. Hence, the problem is reduced to obtaining the composite conductivity and charge carrier mobility, μ. In addition, the electrical conductivity, σ, of many materials including organic, polymer, and crystal materials can be obtained as the sum of the direct-current (DC) and alternating-current (AC) conductivity (i.e., $\sigma = \sigma_{DC} + \sigma_{AC}$).[43,44] The DC conductivity (σ_{DC}) of the composites can be calculated from the *I–V* characteristic curve using the relation[45]

$$\sigma_{DC} = \frac{IL}{VA}. \tag{7}$$

On the other hand, impedance spectroscopy can be used to measure the AC conductivity and dielectric properties of the MSM structure, being employed here in the frequency range from 10^2 Hz to 10^5 Hz. Therefore, the latter method has been used to obtain parameters such as the dielectric permittivity or dielectric constant (ε'), dielectric loss (ε''), and dissipation factor ($\tan\delta$) as functions of frequency.[46] It is well known that the dielectric constant can be written as a complex number, i.e., $\varepsilon = \varepsilon' - i\varepsilon''$, where the imaginary and real parts can be calculated from the following equations[47]:

$$\varepsilon' = \frac{Z''}{\omega\varepsilon_0 \frac{A}{L} Z^2}, \tag{8a}$$

$$\varepsilon'' = \frac{Z'}{\omega\varepsilon_0 \frac{A}{L} Z^2}, \tag{8b}$$

where ω (=$2\pi f$) is the angular frequency of the applied electric field, f is the measured frequency, and Z' and Z'' are the real and imaginary parts of the impedance Z measured at frequency f. Finally, the AC conductivity (σ_{AC}) can be obtained from the above data using the following relation[47]:

$$\sigma_{AC} \approx \omega\varepsilon_0\varepsilon' \tan\delta = \omega\varepsilon_0\varepsilon'', \tag{9}$$

where $\tan\delta$ is the ratio of ε'' and ε'. To estimate the mobility, the space-charge-limited current (SCLC) mechanism for sandwich contacts (such as the MSM system) was employed, being the method commonly

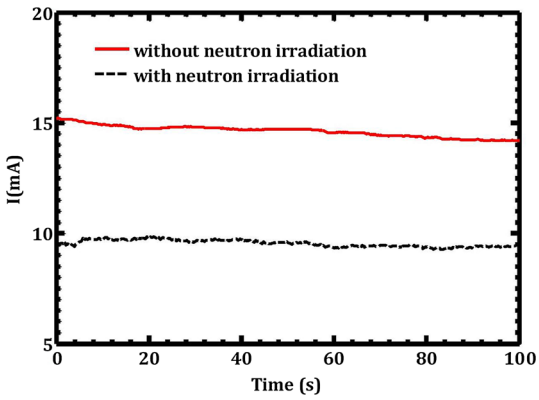

Fig. 10. *I–t* curve for V = 1 V.

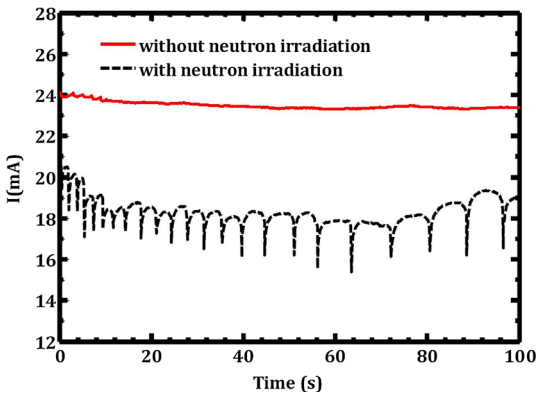

Fig. 11. *I–t* curve for V = 1.8 V.

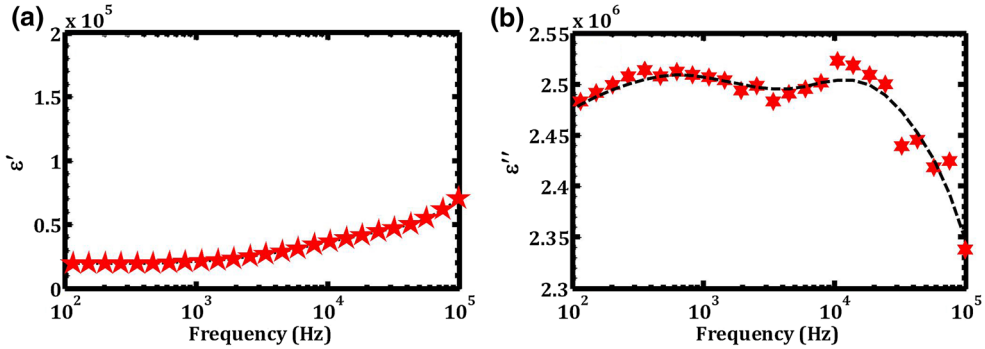

Fig. 12. (a) Real and (b) imaginary parts of complex permittivity of MWCNT/PE composite as function of frequency.

used in organic semiconductor-based electronics.[48] Then, the charge carrier mobility, μ, is given by the equation[49,50]

$$\mu = \frac{8}{9}\frac{1}{\varepsilon_0 \varepsilon} L^3 \left(\frac{\partial \sqrt{J}}{\partial V}\right)^2, \qquad (10)$$

where L is the distance between the two electrodes (channel length).

RESULTS AND DISCUSSION

The effect of different durations of *in situ* neutron irradiation on the *I–V* characteristics of the described MSM system was studied. The results obtained for different irradiation durations are shown in Fig. 8, which can be explained based on the energy band diagrams in the irradiated and nonirradiated conditions. Figure 9 schematically describes the proposed radiation-induced effect on the *I–V* characteristics of the MSM structure.

It is assumed that the positive charges in the HDPE layer, created along the path of proton recoil, induce positive trap charges at the top of the HDPE layer and that conduction electrons combine with holes at the HDPE/(MWCNT/HDPE) interface.[51] This will change the concentration of conduction electrons, raising the conduction band. Therefore, the current flow in the MWCNT/HDPE channel is decreased due to the wider energy bandgap.[13] Additionally, one of the main reasons for current reduction in carbon nanoparticle (CNP)-based Schottky diode is the scattering of electrons in CNPs strain by beta-ray irradiation.[17]

On the other hand, the current also reduces with increasing irradiation time, as shown in Fig. 8. It is clear that the concentration of positive trap charges increased simultaneously as the neutron irradiation time was increased.

The two *I–t* curves shown in Figs. 10 and 11 were obtained in conditions with and without neutron irradiation. Figure 10 shows the results for bias voltage of V = 1 V, while Fig. 11 presents the same results for bias voltage of V = 1.8 V.

Detection of charged energetic particles, e.g., recoiled protons from neutrons, using Schottky diodes has been reported.[52,53] The Schottky diode detects charged particles by collecting electron–hole pairs generated along the path of the particle in the depletion region. Therefore, the detector produces a pulse whose amplitude is proportional to the collected charge. The amount of charge collected may be less than the charge generated in the depletion region due to electron–hole recombination and charge trapping. These effects can be reduced by appropriate selection of the detector material and increasing the intensity of the electric field in the depletion region.

Figure 12 illustrates the variation of ε' and ε'' with frequency for the MSM structure. On the basis of depletion region considerations (Sect. 3.4), the results highlight full depletion of the composite layer, where the width of the depletion region is attained at the threshold voltage where current pulses start ($V_{th} \cong 1.8$ V). Therefore, the MSM structure can be regarded as a capacitor under sufficiently large bias voltage. Moreover, the full depletion region of the organic semiconductor-based MSM system was reported.[54]

CONCLUSIONS

Two Schottky contacts were fabricated using an MWCNT/HDPE composite between two identical copper electrodes. SEM images and the IR spectrum of the synthesized nanocomposite were used for morphological characterization, and the device *I–V* characteristics were measured before and after neutron irradiation. The effect of neutron irradiation on the MWCNT/HDPE-based metal–semiconductor–metal structure was studied. The *p*-type back-to-back Schottky diodes were modeled using thermionic emission theory. The built-in potential, V_{bi}, of the MSM structure was estimated from the experimental *I–V* curve by fitting the ln(J) versus V curve using Eq. 6. Furthermore, the charge carrier mobility was obtained from the *I–V* curve using the SCLC methodology, and the dielectric constant and charge concentration were estimated. Finally, on the basis of impedance measurement results and analytical calculations, a full depleted layer was obtained for the MSM structure. The maximum energy of detectable neutrons was obtained, lying in

the energy range of 7 MeV to 8 MeV, by using the effective sensitive area of the device. The results demonstrate that nanostructured materials can be applied in shield designs for radiation protection applications.

ACKNOWLEDGEMENT

The first author would like to thank Dr. Davod Seifzadeh at the Applied Chemistry Department of University of Mohaghegh Ardabili for his technical support and providing facilities.

REFERENCES

1. T. Reimer, I. Paulowicz, R. Röder, S. Kaps, O. Lupan, S. Chemnitz, W. Benecke, C. Ronning, R. Adelung, and Y.K. Mishra, *ACS Appl. Mater. Interfaces* 6, 7806 (2014).
2. D. Gedamu, I. Paulowicz, S. Kaps, O. Lupan, S. Wille, G. Haidarschin, Y.K. Mishra, and R. Adelung, *Adv. Mater.* 26, 1473 (2014).
3. D.K. Avasthi, Y.K. Mishra, D. Kabiraj, N.P. Lalla, and J.C. Pivin, *Nanotechnology* 18, 125604 (2007).
4. C.L.L. Chen, K. Liu, C. Meng, H. Chunhua, J. Wang, and S. Fan, *ACS Nano.* 5, 1588 (2011).
5. P. Avouris, Z. Chen, and V. Perebeinos, *Nat. Nanotechnol.* 2, 605 (2007).
6. Y. Zhu, H.I. Elim, Y.L. Foo, T. Yu, Y. Liu, W. Ji, J.Y. Lee, Z. Shen, A.T.S. Wee, J.T.L. Thong, and C.H. Sow, *Adv. Mater.* 18, 587 (2006).
7. Z. Spitalsky, D. Tasis, K. Papagelis, and C. Galiotis, *Prog. Polym. Sci.* 35, 357 (2010).
8. J. Kim, S.M. Hong, S. Kwak, and Y. Seo, *Phys. Chem. Chem. Phys.* 11, 10851 (2009).
9. W.-S. Tung, V. Bird, R.J. Composto, N. Clarke, and K.I. Winey, *Macromolecules* 46, 5345 (2013).
10. W.-S. Tung, N. Clarke, R.J. Composto, and K.I. Winey, *Macromolecules* 46, 2317 (2013).
11. T.H. Kim, B.Y. Lee, J. Jaworski, K. Yokoyama, W.J. Chung, E. Wang, S. Hong, A. Majumdar, and S.W. Lee, *ACS Nano.* 5, 2824 (2011).
12. I. Childres, L.A. Jauregui, M. Foxe, J. Tian, R. Jalilian, I. Jovanovic, and Y.P. Chen, *Appl. Phys. Lett.* 97, 173109 (2010).
13. T.-Y. Kim, K. Cho, W. Park, J. Park, Y. Song, S. Hong, W.-K. Hong, and T. Lee, *ACS Nano.* 8, 2774 (2014).
14. T. Susi, J. Kotakoski, R. Arenal, S. Kurasch, H. Jiang, V. Skakalova, O. Stephan, A.V. Krasheninnikov, E.I. Kauppinen, U. Kaiser, and J.C. Meyer, *ACS Nano.* 6, 8837 (2012).
15. W.K. Hong, G. Jo, J.I. Sohn, W. Park, M. Choe, G. Wang, Y.H. Kahng, M.E. Welland, and T. Lee, *ACS Nano.* 4, 811 (2010).
16. S. Kim, S. Lee, and J. Hong, *ACS Nano.* 8, 4698 (2014).
17. H. Kasani, M. Taghi Ahmadi, R. Khoda-bakhsh, D. RezaeiOchbelagh, and R. Ismail, *J. Appl. Phys.* 119, 124510 (2016).
18. M. Foxe, G. Lopez, I. Childres, R. Jalilian, A. Patil, C. Roecker, J. Boguski, I. Jovanovic, and Y.P. Chen, *IEEE Trans. Nanotechnol.* 11, 581 (2012).
19. M. Foxe, E. Cazalas, H. Lamm, A. Majcher, C. Piotrowski, I. Childres, A. Patil, Y.P. Chen, and I. Jovanovic, *In: Nuclear Science Symposium and Medical Imaging Conference (NSS/MIC), 2011 IEEE*, (IEEE: 2011), pp 352–355.
20. H. Gotoh and H. Yagi, *Nucl. Instrum. Methods* 101, 395 (1972).
21. T.M. Filho, M.M. Hamada, F. Shiraishi, and C.H. de Mesquita, *Nucl. Instrum. Methods Phys. Res. A* 458, 441 (2001).
22. A. Šagátová-Perd'ochová, F. Dubecký, B. Zaťko, I. Chodák, M. Ladzianský, and V. Nečas, *Nucl. Instrum. Methods Phys. Res. A* 576, 56 (2007).
23. G.F. Knoll, *Radiation Detection and Measurement* (Hoboken: Wiley, 2010).
24. N.A. Bakh, A.V. Vannikov, A.D. Grishina, and S.V. Nizhnii, *Russ. Chem. Rev.* 34, 736 (1965).
25. W. Liu, Y. Miao, and Q. Meng, *Integr. Ferroelectr.* 138, 77 (2012).
26. W. Ding, A. Eitan, F.T. Fisher, X. Chen, D.A. Dikin, R. Andrews, L.C. Brinson, L.S. Schadler, and R.S. Ruoff, *Nano Lett.* 3, 1593 (2003).
27. T.R. Fadel, F.A. Sharp, N. Vudattu, R. Ragheb, J. Garyu, D. Kim, E. Hong, N. Li, G.L. Haller, L.D. Pfefferle, S. Justesen, K.C. Herold, and T.M. Fahmy, *Nat. Nanotechnol.* 9, 639 (2014).
28. E. Celia, E.T. de Givenchy, S. Amigoni, and F. Guittard, *Soft Matter* 7, 10057 (2011).
29. C. Cunha, S. Panseri, D. Iannazzo, A. Piperno, A. Pistone, M. Fazio, A. Russo, M. Marcacci, and S. Galvagno, *Nanotechnology* 23, 465102 (2012).
30. L. Stobinski, B. Lesiak, L. Kövér, J. Tóth, S. Biniak, G. Trykowski, and J. Judek, *J. Alloys Compd.* 501, 77 (2010).
31. S. Goyanes, G.R. Rubiolo, A. Salazar, A. Jimeno, M.A. Corcuera, and I. Mondragon, *Diam. Relat. Mater.* 16, 412 (2007).
32. J. Chiquito Adenilson, A. Amorim Cleber, M. Berengue Olivia, S. Araujo Luana, P. Bernardo Eric and R. Leite Edson, *J. Phys. Condens. Matter* 24, 225303 (2012).
33. S.M Sze and K.K Ng, *Physics of Semiconductor Devices*. (Wiley: New York, 2006).
34. H. Elhadidy, J. Sikula, and J. Franc, *Semicond. Sci. Technol.* 27, 015006 (2012).
35. A.A. Mowlavi and R. Koohi-Fayegh, *Appl. Radiat. Isot.* 60, 959 (2004).
36. S. Croft, *Nucl. Instrum. Methods Phys. Res. A* 281, 103 (1989).
37. J.C. Vitorelli, A.X. Silva, V.R. Crispim, E.S. da Fonseca, and W.W. Pereira, *Appl. Radiat. Isot.* 62, 619 (2005).
38. D. Rezaei Ochbelagh, H. Miri Hakimabad, and R. Izadi Najafabadi, *Nuclear Instruments and Methods in Physics Research Section A: Accelerators, Spectrometers, Detectors and Associated Equipment* 577, 756 (2007).
39. T. Bortfeld, *Med. Phys.* 24, 2024 (1997).
40. E.H. Rhoderick and R.H. Williams, *Metal-Semiconductor Contacts* (Oxford: Clarendon, 1978).
41. A. Takshi, A. Dimopoulos, and J.D. Madden, *Appl. Phys. Lett.* 91, 083513 (2007).
42. L. Pintilie and M. Alexe, *J. Appl. Phys.* 98, 124103 (2005).
43. S.R. Elliott, *Physics of Amorphous Materials*. (Longman London; New York, 1983).
44. G. Conte, M.C. Rossi, S. Salvatori, and G. Vitale, *Diam. Relat. Mater.* 13, 891 (2004).
45. N.A. Bhagat, N.K. Shrivastava, S. Suin, S. Maiti, and B.B. Khatua, *Polym. Compos.* 34, 787 (2013).
46. S. Lanfredi and A.C.M. Rodrigues, *J. Appl. Phys.* 86, 2215 (1999).
47. M.H. Al-Saleh, H.K. Al-Anid, Y.A. Husain, H.M. El-Ghanem, and S.A. Jawad, *J. Phys. D Appl. Phys.* 46, 385305 (2013).
48. A. Hajibadali, M. Baghaei Nejad, and G. Farzi, *Braz. J. Phys.* 45, 394 (2015).
49. S.M. Sze, *Physics of Semiconductor Devices*. (Wiley-Interscience, 1969).
50. A.R. Tameev, L. Licea Jiménez, L. Ya Pereshivko, R.W. Rychwalski, and A.V. Vannikov, *J. Phys: Conf. Ser.* 61, 1152 (2007).
51. E. Simoen, A. Mercha, J.M. Rafí, C. Claeys, N.B. Lukyanchikova, A.M. Smolanka, and N. Garbar, *J. Appl. Phys.* 95, 4084 (2004).
52. A.L. Giudice, F. Fasolo, E. Durisi, C. Manfredotti, E. Vittone, F. Fizzotti, A. Zanini, and G. Rosi, *Nucl. Instrum. Methods Phys. Res. A* 583, 177 (2007).
53. W. Jian, M. Li, Y. Jiang, J. Li, Y. Zhang, H. Gao, X. Liu, D. Jinfeng, D. Zou, X. Fan, L. Gan, C. Peng, L. Yi, and J. Lei, *Nucl. Instrum. Methods Phys. Res. A* 771, 17 (2015).
54. C.H. Kim, O. Yaghmazadeh, D. Tondelier, Y.B. Jeong, Y. Bonnassieux, and G. Horowitz, *J. Appl. Phys.* 109, 083710 (2011).